Catalysis Letters
https://doi.org/10.1007/s10562-020-03221-z

Square CdS Micro/Nanosheets as Efficient Photo/Piezo-bi-Catalyst for Hydrogen Production

Hayder A. Abbood[1,2] · Akram Alabadi[3] · Adnan B. Al-Hawash[4] · Anwar A. Abbood[1,2,3,4,5] · Kaixun Huang[1,2]

Received: 31 January 2020 / Accepted: 14 April 2020

Abstract

Cadmium sulfide (CdS) is a member of an important subgroup of two-dimensional (2D) transition metal dichalcogenides that can promote a number of useful oxidation reactions under visible light and ultrasonic vibrations. Herein, we report a low-cost hydrothermal method assisted by DL-dithiothreitol for controlling the thickness of CdS nanosheets. In particular, square-like CdS nanosheets with a thickness of 28 nm were acquired at a molar ratio of 2:1 of DL-dithiothreitol to a cadmium source. Furthermore, a significant connection was observed between CdS nanosheet thickness and photocatalytic H_2 evolution. Thin square nanosheets exhibited high photocatalytic activity under the combination of light and vibrational energy. These nanosheets can be assigned to active sites due to an increase in surface area and can induce a piezoelectric field in CdS via ultrasound. Thickness differences exert a critical synergy effect on photo/piezo-bi-catalyst performance. The thinnest product achieved the maximum photocatalytic H_2 production yield (1293.62 μmol g^{-1} h^{-1}), which is approximately 4.2 times that of the 0-CdS micro-sheets (284.26 μmol g^{-1} h^{-1}). This report illustrates the effect of CdS nanosheet thickness on photo/piezo-bi-catalytic H_2-production operation and provides inspiration for engineers to develop high-efficiency two-dimension photocatalysts.

Graphic Abstract

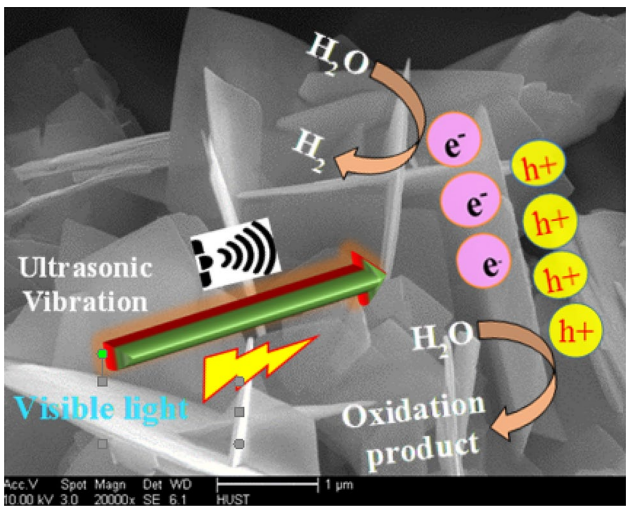

Keywords Photo/piezo-bi-catalysis · CdS · Hydrogen photogeneration · Two-dimension nanosheets · Thickness control

Electronic supplementary material The online version of this article (https://doi.org/10.1007/s10562-020-03221-z) contains supplementary material, which is available to authorized users.

Extended author information available on the last page of the article

Published online: 22 April 2020

1 Introduction

Photocatalytic water splitting is considered the most promising solution to energy storage and clean fuel production [1]. Since the pioneering work of Fujishima and Honda on the H_2 evolution of titanium dioxide (TiO_2) electrodes utilizing ultraviolet (UV) light in 1972 [2], numerous organic and inorganic semiconductor materials have been presented for photocatalytic H_2-evolution and water decomposing [3, 4]. To maximize the use of visible-spectrum zones in sunlight, cadmium sulfide (CdS)with a perfect position of the conduction band edge and acceptable band gap (2.42 eV) was considered an outstanding visible-light-responsive material for hydrogen generation under solar energy [5–7]. Considerable advances have been attained in the area of CdS photocatalysts fabrication such as, nanoparticles [8], quantum dots [9, 10], nanowires [11, 12], nanorods [13, 14], nanotube [15, 16], and nanosheets [17, 18]. However, the rational design of effective and reliable CdS-based H_2-evolution systems for practical applications remains a huge challenge due to poor separation ability of excited electron and hole charges, unwanted photo-generated hole-driven deactivation processes [19] and effect of the photo-corrosion [5, 20]. Accordingly, a wide range of modification methods, including constructing hetero-junction semiconductor [21, 22], the fabricating Z-scheme systems [23, 24], loading of cocatalysts [25, 26], coupling of nano-carbons [27, 28] and surface doping [29], have been suggested over the last few decades to vastly improve the stability and photoactivity of CdS in generating H_2. However, the drawbacks of hybrid photocatalyst techniques are evident compare with the statistics of single photocatalyst components. With the exception of the costs regularly used of noble metals, the relatively inactive charge transport between components via interfaces is also undesirable [30]. Therefore, optimized green routes for the direct separation of (e^-–h^+) on the best of narrow or deformation-band gap photocatalysts should be further developed [31].

At present, the piezo-phototronic effect or the localized electric field can play a essential role in photocatalytic performance by producing electric charges on the surface of single-component piezo-catalysts [32, 33]. Moreover, acoustic energies can make electrons and holes move in contrary directions to the materials surface [34, 35] and recombination of (e^-– h^+) be more lifetime [36]. In this regard, the noncentral symmetric crystal wurtzite structure of CdS is a typical piezoelectric semiconductor that can produce an internal electric field under light and strains, inducing the separation of photogenerated electrical charges [37]. Otherwise, given that 2D nanosheets have a unique morphology, they deform easily due to the action of external forces enhancing the piezoelectric effect [38]. Ping groups recently suggested that the ultrasound-induced piezoelectric field in CdS leads to more facile water destruction for H_2 production than visible-light illumination alone [39]. Yan et al. demonstrated that the application of dual-stimuli ultrasonic light to ultrathin CdS nanosheets improves their photocatalytic H_2-evolution due to a photo-acoustic synergetic mechanism [40]. Nevertheless, the influence of ultrasonic vibration on the irregular in shapes and in sizes of nanosheets remains unclear [7].

Herein, an environment friendly and cost-effective hydrothermal approach was used to synthesize 2D square-like CdS nanosheets. The thickness of the CdS nano sheets can be easily adjusted by altering the amount of DL-dithiothreitol which functions as a structural-directing agent in the as-prepared system. In addition, the formation mechanism of the square-like CdS nanosheets was suggested and the influence of thickness on the efficiency of photocatalytic water cracking was studied. The more slimmest sheets sample showed optimum photocatalytic H_2 generation performance (1293.62 μmol g^{-1} h^{-1}) with a quantum efficiency of 11.72% at a visible wavelength of 440 nm under the coupling of light irradiation and ultrasonic vibration, This generation performance was approximately 4.5-fold that of the 0-CdS sample (284.26 μmol g^{-1} h^{-1}) and higher than those of the other thicker CdS sheet samples. The current study presents an easy and direct technique for preparing a square like CdS nanosheets with superbly regulated thickness and highlights the thickness influence of their activity during photocatalytic H_2 production.

2 Experimental Section

2.1 Chemicals

Cadmium sulfate hydrate (≥ 99.0%), CH_4N_2S (≥ 99.0%) DL-dithiothreitol, ammonium hydroxide, methanol, glycerin, lactic acid, sodium sulfide (≥ 99.0%), sodium sulfite, (≥ 99.0%), and H_2PtCl_6. $6H_2O$, were purchased from Shanghai Chemical Reagent Co., China. The other chemicals utilized in this study were of analytical grade and used as received without any further treatment.

2.2 Prepare of 2D Square-Like CdS Nanosheets

The 2D square-like CdS nanosheets were fabricated using a simple hydrothermal process. In a typical experiment, Cadmium sulfate hydrate solution (15 mL, 0.2 M) was added drop by drop to a clear water solution of DL-Dithiothreitol (4 mmol, 20 mL) and sonicated for 15 min. Then, 3 mL of 20% ammonium hydroxide and 5 mL of 1.2 M thiourea solutions were quickly poured sequentially. After vigorous

stirring for about 45 min, the above solution was transferred to 50 mL Teflon lined steals autoclaves and kept at 180 °C for 12 h. After naturally cooling, the yellow product was collected by centrifugation, rinsed several times by distilled water and ethanol, and dried in a vacuum oven at 50 °C for 24 h and denoted as 6-CdS. Due to changes in dimensioning of samples by varying amounts of DL-dithiothreitol, the nanosheets fabricated by adding 0, 2, 4, and 6 mmol of DL-dithiothreitol were denoted as 0-CdS, 2-CdS, 4-CdS, and 6-CdS.

2.3 Sample Characterization

The results were examined using an X-ray powder diffractometer (PANalytical χ' Pert Pro, the Netherlands) equipped with Cu Kα radiation (λ = 1.5418 Å) at a scanning rate of 0.02° s^{-1} within a 2θ range of 5–90°. The other equipment used included a field emission scanning electron microscopy(SIRION 200), an energy-dispersive X-ray spectrometer attached to the field emission scanning electron microscopy (FESEM) system, a transmission electron microscopy (Tecnai G220), a high-resolution transmission electron microscopy (JEM-2010FEF TEM), an X-ray photoelectron spectrometer (AXIS-ULTRA DLD high- performance imaging, Shimadzu, Japan), a Brunauer–Emmett–Teller (BET) Micromeritics ASAP2020M Surface Area and porosity analyzer, and a UV–Visible (UV–Vis) spectrophotometer (Shimadzu, no. 2450).

2.4 *Photocatalytic H_2 Evolution*

Photocatalytic water cracking was determined using a Pyrex reactor equipped with an evacuation system and closed gas circulation. First 50 mg of the photocatalyst was suspended in a sealed 100 mL Pyrex flask containing 80 mL of lactic acid as the sacrificial agent under continuous stirring. The aqueous solution of $H_2PtCl_6.6H_2O$ was added dropwise to the system to produce 1 wt% platinum loading on the fabricated samples by using a photochemical reduction deposition process. Prior to applying irradiation by using a lamp with a UV cut-off filter (λ ≥ 420 nm) and bottom sonication by using a 100 W ultrasonic generator, the Pyrex reactor was degassed to remove dissolved oxygen and then sealed. The experiment was carried out at room temperature and the light intensity was 0.8846 mW/cm^2. The solution was exposed to light for 3 min and placed under strain provided by the ultrasonic vibration source for 3 min during piezo-/photo-bi-catalysis. The amount of evolved H_2 was assessed using an online gas chromatograph (GC7890II, Tianmei, Shanghai; nitrogen carrier gas) with a thermal conductivity detector.

3 Results and Discussion

3.1 Analysis of Phase Structure

The X-ray pattern of the CdS nanosheets fabricated through the hydrothermal process is shown in Fig. 1. Evidently, the pure hexagonal CdS fibrous mineral structure (JCPDS Card, No.41–1049) with lattice constants a = 0.4141 nm, and c = 0.6716 nm was only attained for the 2-CdS and 4-CdS samples. No peaks on these X-ray diffraction (XRD) curves match the other CdS phase. The X-ray pattern of 0-CdS nanosheets indexed a trace of a phase transition to the zinc blend CdS phase. The XRD pattern of the 6-CdS sample exhibits series of peaks at 2θ 23.888, 36.28, 40.04 and 49.67 confirming that S was predicted in this sample. The low amount of DL-dithiothreitol has no changing effect on the crystal phase of CdS nanosheets compared with those observed in the 0-CdS and 6-CdS samples. The energy-dispersive X-ray spectroscopy (EDS) analysis result confirmed that the 4-CdS sample is composed mostly of two elements, Cd and S, with molar ratio of 1.009:1 (Fig. SI, Supporting Information).

3.2 FESEM and Transmission Electron Microscopy (TEM)

A field emission scanning electron microscopy (FESEM) technique was used to examine products morphology. Figure 2a–c show the FESEM images of the 4-CdS products fabricated at 180 ºC with 4 mmol of dithiothreitol. The products exhibit square nanosheets with uniform thickness (approximately 28.83 nm), and the width or length are ranges from 500 nm to 3 µm for small and large scales nanosheets. Moreover, most of these nanosheets aggregated to form a hierarchical structure and typically have smooth

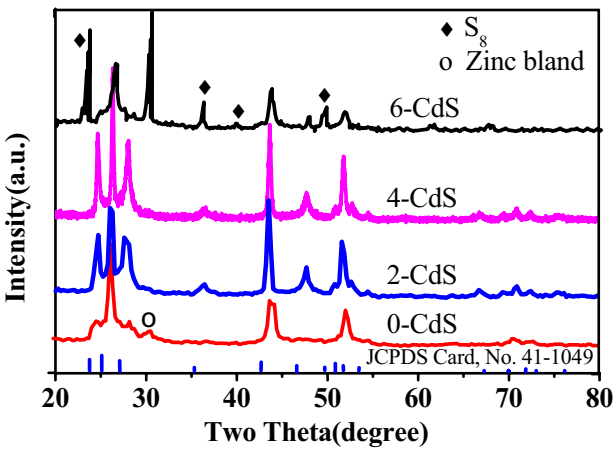

Fig. 1 XRD patterns of 0-CdS, 2-CdS, 4-CdS and 6-CdS samples

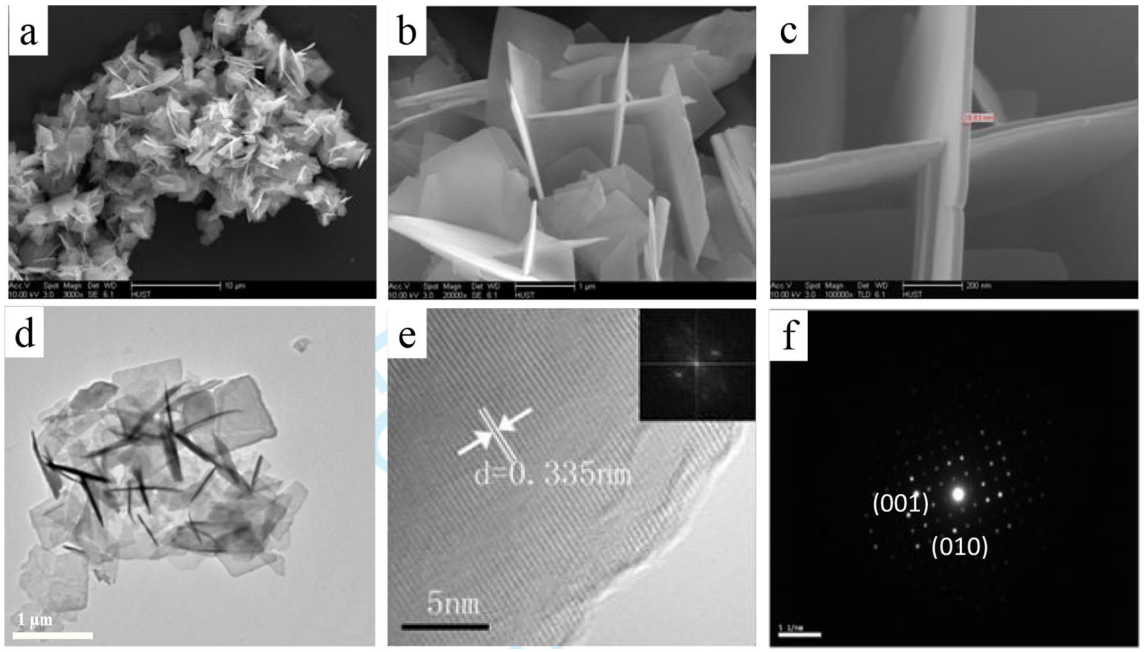

Fig. 2 FESEM images of the square 4-CdS nanosheets fabricated by a hydrothermal process at 180 °C for 12 h. **a** and **b** Low-magnification FESEM image; **c** close-up view of single cross structure; **d** TEM image square 4-CdS nanosheets; **e** HRTEM image of single nanosheets inset with FFT pattern; **f** SAED pattern

and flat surfaces, that differ from those observed in bismuth oxyiodide (BiOI) [41]. The square nanosheets were further checked using TEM and high-resolution TEM (HRTEM). Figure 2d–f show the TEM images of the square 4-CdS nanosheets. A low-fold transmission electron microscope (Fig. 2d) shows that the nanosheet structure highly agrees with the FESEM results. The HRTEM images (Fig. 2e) indicate that the lattice spacing of nanosheets 0.335 nm, which attributable to the wurtzite structure of the CdS (002) crystal plane. This result shows that the (001) orientation is the preferential growth direction of the nanosheets, which agrees with the XRD results. In addition, the inset fast Fourier transform (FFT) image proves that the (001) direction is the preferred orientation. The selected area electron diffraction pattern (SAED) of the as-prepared crystal in Fig. 2f shows that the nanosheet is depicted as a single crystal and the diffraction spot can be indexed to CdS with a hexagonal structure. This result is supported by the FFT pattern (Fig. 3e, inset). Furthermore, Fig. SII (Supplementing Information) shows the FESEM images when reaction time changes and dithiothreitol concentration remains equal to 4 mmol with the same remainder as the other reaction conditions.

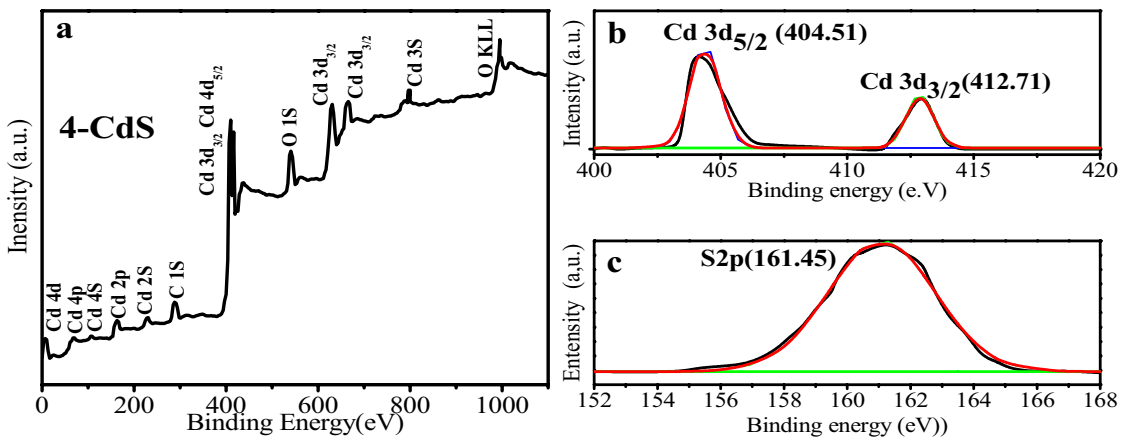

Fig. 3 XPS spectra of 4-CdS sample: **a** full spectrum, **b** Cd 3d, **c** S 2p

3.3 X-ray Photoelectron Spectroscopy (XPS) Analysis

The *XPS* technique was performed to determine the chemical compositions and oxidation state of an element in 4-CdS. The Cd, S and the background patterns of carbon 1 s and oxygen 1 s were directly observed in the typical survey spectrum (Fig. 3a). The major doublets signal centered at binding energies 404.51 (cadmium 3d5/2) and 412.71 eV (cadmium 3d3/2) in the high-resolution XPS spectra are the characteristics of Cd^{2+} (Fig. 3c) [42]. The signals at 161.45 (sulfur 2p1/2) and 224.89 eV (sulfur 2p3/2) in Fig. 3a and 3c are due to the spin–orbit doublets of S^{2-} in 4-CdS [43, 44]. No peaks at binding energies 164 eV and 167–169 eV indicate that 4-CdS is clearly from sulfur element and sulfur oxides. This finding established the presence of a sulfur elements in S^{-2} form in this sample. Moreover, no characteristic peaks of cadmium sulfate were perceived, suggesting that the starting material $CdSO_4.8/3H_2O$ was completely converted to CdS sheets during the 12 h hydrothermal process at 180 ℃. On the basis of these results, they are consistent with the phase purity and crystallographic structure of X-ray patterns in compared with the fabricated 4-CdS (Fig. 1), indicating that 4-CdS was positively synthesized.

3.4 Optical Property Analysis

The optical absorption characteristics of the fabricated samples 0-CdS, 2-CdS, 6-CdS, and 6-CdS were examined using diffuse reflectance UV–Vis spectroscopy. As shown in Fig. 4a, the notable increase in absorption close to the wavelength of 550 nm is associated with the intrinsic bandgap absorption of cadmium sulfide [45, 46]. Remarkably, the absorption edge exhibited a shift to a higher wavelength when the amount of DL-dithiothreitol was regularly increased from 0 to 4 mmol. This shift can be related to the effect of the specified quantum size occurring from the products with minimized thickness from 0-CdS to 4-CdS [47]. By contrast, the absorption edge demonstrated a shift to a lower wavelength when the amount of DL-dithiothreitol exceeded 4 mmol. This outcome is sensible because the thickness of the 2D CdS nanosheets increase beginning with the 4-CdS product, concurring with the thickness propensity considered earlier. Moreover, Fig. 4 indicates that the energy band gaps value of the 4-CdS, 2-CdS, 0-CdS, and 6-CdS products calculated using (Kubelka–Munk formula [48] are 2.24, 2.3, 2.36 and 2.41 eV, respectively.

3.5 Photoluminescence (PL) Analysis

The PL spectrum peak at an excitation wavelength of 380 nm is depicted in Fig. 5 to explore the (e^-–h^+) pair's recombination of the CdS nanosheets. The radiative recombination of electron–hole plasma in CdS sheets is clearly shown in the PL emission peak at 444 nm. The intensity of this peak initially increased (0 -CdS) and then move back when the dosages of DL-dithiothreitol increased from 2 to 4 mmol. In particular, its intensity was maximized in the 6-CdS investigating this situation, the same behavior was observed with thickness. That is, thin CdS nanosheets can output photo-generated (e^-–h^+) pairs supplied by active atoms on the surface, which decreasing recombination probability and PL emission peaks.

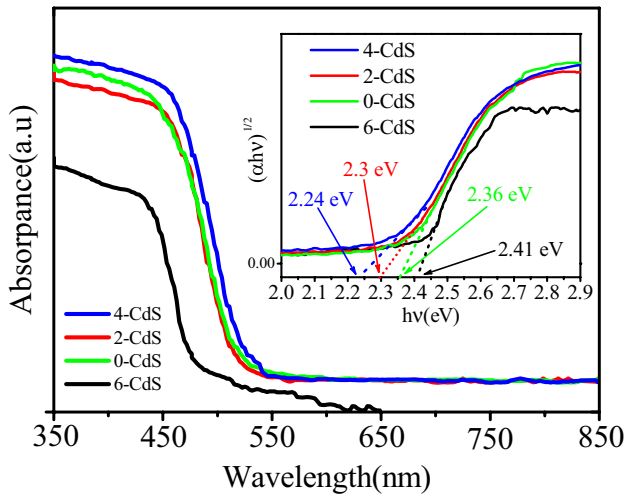

Fig. 4 UV–Vis diffuse reflectance spectra for synthesized sample, inserted plots Kubelka – Munk function versus photon energy curves

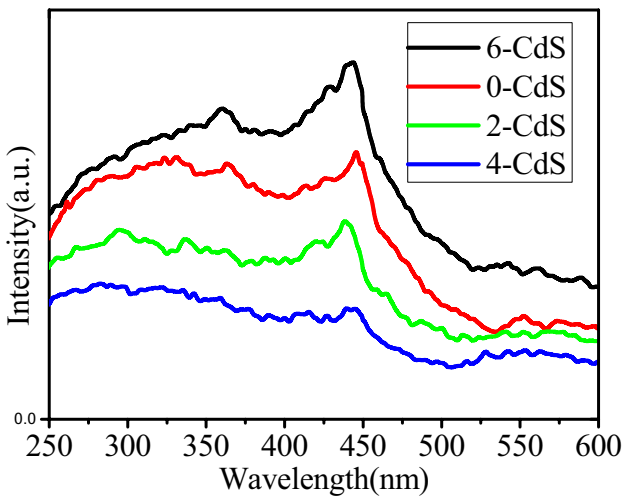

Fig. 5 PL spectrum of the all prepared CdS samples

3.6 Mechanism Growth of CdS Nanosheet

During the formation of 2D CdS nanosheets, the reaction rate between cadmium ion Cd^{2+} and sulfide ion S^{2-} was adjusted using water and ammonia as a complexion agent (forming a complex by coordinating Cd^{2+} ion with water and NH_3 produced form decomposing thiourea) to release Cd^{2+} gradually. Thereafter, thiourea slowly dissociated in hydrothermal alkaline solution to release ammonia and S^{2-} (Fig SIII, Supporting Information). CdS nuclei are normally formed after thiourea decomposition, and these pre- nucleated seeds begin to grow into varied crystal polymorphs, shapes, and sizes to form various nanostructures after the nucleation stage because of the sulfidation effect. In this report, DL-dithiothreitol was adsorbed on the surface of the CdS nucleus, operating as the structure agent-director for lateral secondary growth. The surfaces of CdS nuclei and DL-dithiothreitol are characterized as polar surfaces and with high surface energy for the regrowth of other cadmium surface CdS nanostructures. Thus, the CdS microstructure is restricted using DL-dithiothreitol, and achieving two-dimension nanosheets growth steps series can be interpreted using the following chemical equation:

Firstly, the hexaaqua-cadmium (II) complex is formed via the reaction between water solvent and Cd^{2+},

$$Cd^{2+} + 6H_2O \rightarrow \left[Cd\left(H_2O\right)_6\right]^{2+} \quad (1)$$

Then, thiourea is decomposed in alkaline media to slowly release NH_3 and S^{2-} ions,

$$CH_4N_2S + NH_4OH \rightarrow H_2S + NH_3 + CN_2H_2 + H_2O \quad (2)$$

By contrast, cadmium-ammonia complex ions may form due to an increase of in ammonia concentration,

$$Cd^{2+} + 4NH_3 \rightarrow \left[Cd\left(NH_3\right)_4\right]^{2+} \quad (3)$$

Lastly, CdS is produced when sulfide ions are shared with hexaaqua–cadmium (II) and cadmium-ammonia complex ions,

$$\left[Cd\left(H_2O\right)_6\right]^{2+} + S^{2-} \rightarrow CdS \quad (4)$$

$$Cd\left(NH_3\right)_4]^{2+} + S^{2-} \rightarrow CdS \quad (5)$$

3.7 CdS Nanosheet Thickness

The effect of DL-dithiothreitol amounts on the thicknesses of CdS nanosheets was further explored using by FESEM. As shown in Fig. 3a–c the thickness of the 0-CdS sample sheet without DL-dithiothreitol is approximately 311.39 nm. Moreover, Fig. 6d, f and j–l show that the thicknesses of the 2-CdS, 4-CdS, and 6-CdS samples are approximately 38, 28.83 and 93.73 nm, respectively. This decrease in the thickness of nanosheets can provide a wider area of uncovered atoms on the surface for UV–Vis light energy harvesting, while the use of incident photons is difficult for the interior atoms of the thicker nanosheets, and a portion of the energy incident photons is confined the crystal at the internal grain boundaries crystal, causing low light utilization [49]. Moreover, the photogenerated e^- movement range in the thinner nanosheets is shortened. Thus, the transfer and separation of photogenerated electron—hole pairs are enhanced. Consequently, the implementation of photocatalytic H_2 generation is highly endorsed [50]. The thickness of the cadmium sulfide nanosheets decreases with the amount of DL-dithiothreitol and returns to the early case, which can be ascribed to the construction mechanism suggested earlier. The promotion and suppression effect are two opposite trends that meet in an intermediate. Arbitrary growth is stunt with a controlled quantity of DL-dithiothreitol and the increasing dose leads to additional nucleation sites. Furthermore, a similar impact of DL-dithiothreitol measurement was observed on particular surface regions measured using Brunauer-Emmett and Teller (BET). This results for 0-CdS, 2-CdS, 4-CdS, and 6-CdS are 8.37, 22.92, 38.95 and 16.62 m^2/g respectively. The large BET of the 4-CdS sample provides it with abundant active sites for the photodecomposition of H_2O. The measurements of nitrogen adsorption and desorption and the related Barrett–Joyner–Halenda curves for pore size distribution were performed on 2-CdS and 4-CdS-6 as shown in Fig. SVI (Supporting Information).

3.8 Photocatalytic Activity and Mechanism

The photocatalytic hydrogen evolution activities of the 0-CdS, 2-CdS, 4-CdS and 6-CdS sheets with 1 wt% platinum was evaluated under photo-/piezo-bi-catalysis using 80 mL of 10% lactic acid as sacrificial agent, as present in Fig. 7. Under visible light illumination condition, the control tests show that no H_2 output can be detected without irradiation or photocatalysts, indicating that all the as-samples are essential to the development of H_2 production. The overall H_2 production amounts of the as-prepared catalyst during all the photoreactions were measured and presented in Fig. 7a. The control tests in Fig. 7b show that ultrasounds can result in water cracking when generating trace hydrogen without photocatalysts. Moreover, no remarkable change in the hydrogen yield was observed in any of the as-prepared samples, indicating that sound waves can hardly directly increase H_2-evolution, and two-dimension CdS sheets cannot functions as a sono-catalyst. These results are agreed with previous works [51]. However, when ultrasound and

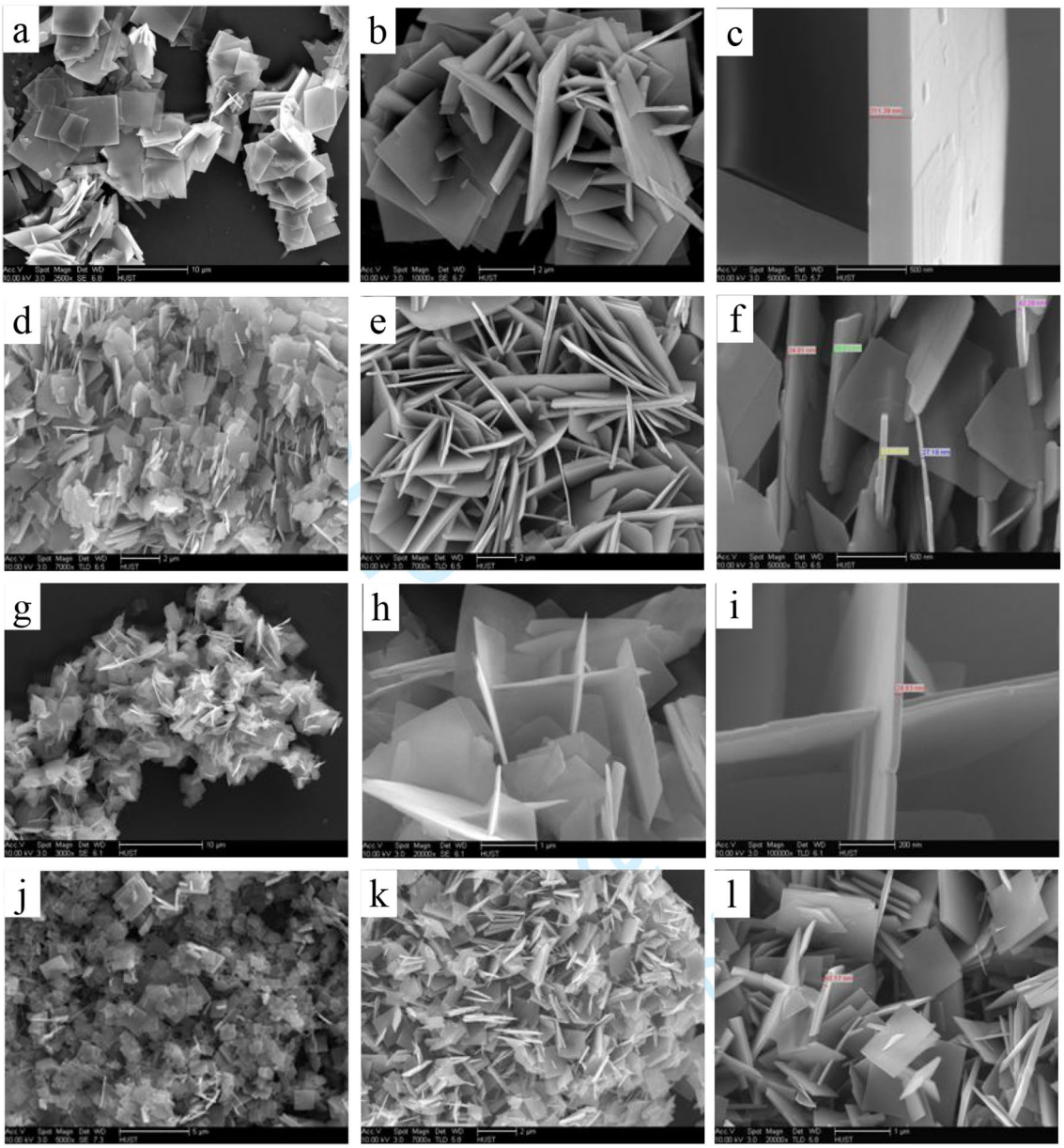

Fig. 6 FSEM images of the as-prepared: **a–c** 0-CdS micro-sheets, **d–f** 2-CdS nanosheet, **g–i** 4-CdS square nanosheet, and **j–l** 6-CdS nanosheets respectively

light simultaneously applied to the photoreaction system, additional H_2 production of all the as-obtained product was apparently detected as shown in Fig. 7c. The amount of hydrogen evolution after 6 h of photoreaction time was collected and displayed in Fig. 7d to compare the piezo-/photo-bi-catalytic application and demonstrate the advantageous impact of two-dimension CdS nanosheet thickness on H_2-generation activity. The amount of hydrogen generated by the 4-CdS photocatalyst was higher than that in the case with the imposition of light and ultrasound vibration. This result occurred because only a proportion of the electrons produced by the photocatalytic process traveled to the surfaces of the as-samples and reacted with water. DL-dithiothreitol dosage plays a direct role in controlling the thickness of CdS sheets, while indirectly affecting the activity of H_2 evolution. The thinnest product, 4-CdS, and 2-CdS, produced the highest amounts of hydrogen of 1293.62 µmol/g h^{-1} and 862.5 µmol/g h^{-1} respectively, which can provide higher reaction rate on the surface through numerous active centers. However, the H_2 generation value beings to decline in the 6-CdS (339.5 µmol/g) and 0-CdS (186.32 µmol/gm) test. To comprehensively explain why CdS nanosheet thickness is increasing as evident from FESEM images (Fig. 2).

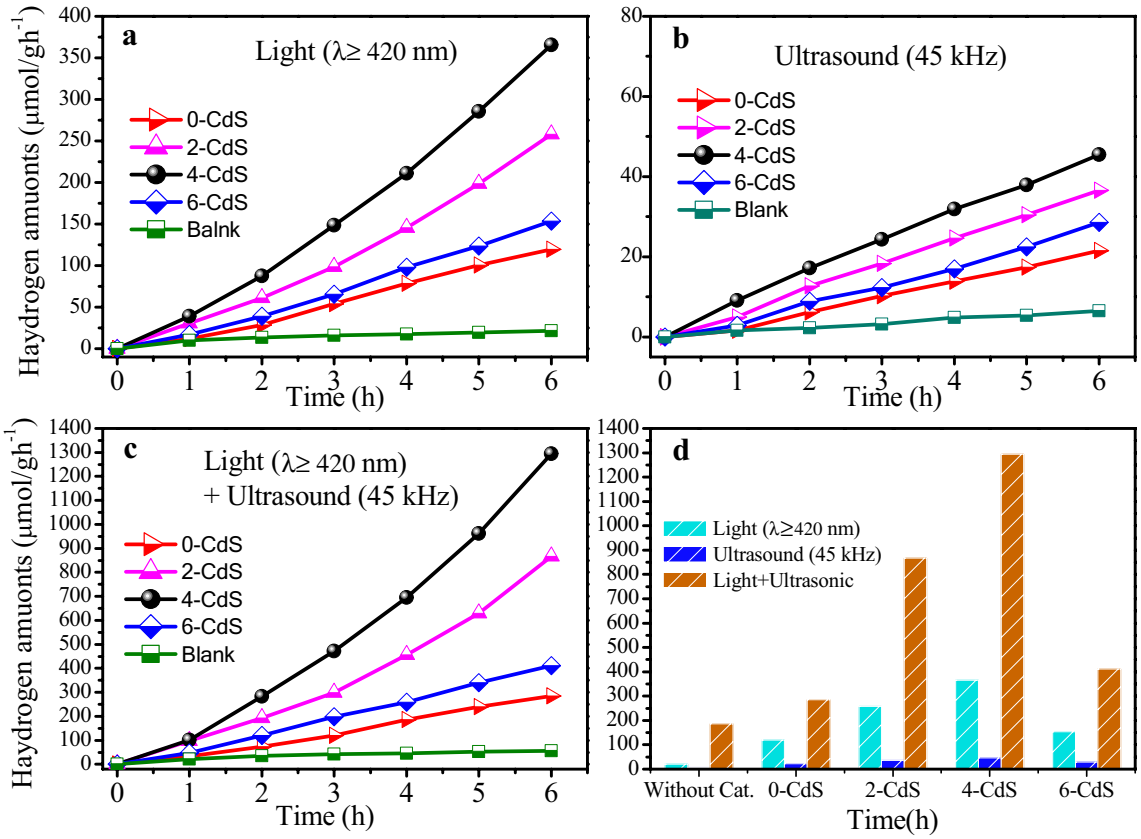

Fig. 7 **a**–**c** Reaction time courses over 0-CdS, 2-CdS, 4-CdS and 6-CdS photocatalysts at different condition in aqueous solution. **d** Comparison of H_2 evolution amounts of all as-prepared samples under various conditions

Considering the effectiveness of the square 4-CdS nanosheets under the influence of light, the combined effects of (light and ultrasound) on water decomposition compared with the other as-prepared materials, and the lack of report on H_2–evolution with pure CdS without any sacrificial agent [52], hydrogen production in the square 4-CdS nanosheets was performed under photocatalysis(light), piezocatalysis (sound), and their simultaneous imposition with various sacrificial agents containing 10% methanol, 10% glycerin, 10% lactic acid and (0.35 M Na_2S, 0.25 M Na_2SO_3). As illustrated in Fig. 8a, the photocatalytic hydrogen evolution of the 4-CdS sample in 10% lactic acid was considerably higher than that of the other sacrificial agents. The hydrogen production trend in the photocatalytic process should follow an ultrasound-frequency-dependent common distribution. The act of synergetic hydrogen production was tested with the same visible-light source at different ultrasonic frequencies (55 kHz, 45 kHz, 55 kHz, and 25 kHz). As shown in Fig. 8b, the amount of hydrogen evolution varies significantly with ultrasonic frequency after sound intensities normalized. Therefore, we assume that the frequency of the prepared nanosheets nearest to the resonance frequency is 45 kHz within the experimental range. In addition, the change trend exhibits normal distribution. Consequently, depending on the results presented above, the photoacoustic H_2-evolution synergy follows the mechanism in which the piezoelectric field induced by ultrasound expedites the photo-generated (e^-–h^+) pairs separation.

Figure 9a shows the hydrogen evolution rate on the 4-CdS sample for 1, 2, 3, 4, 5, 6, 7 and 8 h. The highest rate of H_2-production reached to 215.62 μmol h^{-1} in 6 h photoreaction time. A series of experiments on the H_2-generation and quantum efficiency was performed using monochromatic light illumination to optimize photoactivity over 4-CdS (Fig. 9b). The H_2-evolution rate reached as high as 215.62 μmol h^{-1} and the resulting quantum efficiency was 11.27% below the wavelength of 460 nm. The highest photoactivity was achieved was achieved at a substantial absorption of 440 nm, and photocatalytic efficiency gradual decreased with an increase the of light location of absorption. This result can be attributed to the optimal absorption of light energy by the absence of a light deviation or refraction on the auxiliary surface at wavelengths 440 nm. All the aforementioned results are compatible with the UV–Vis absorption spectra. Cycling experiments were also conducted to verify the long-term stability and repeatability of

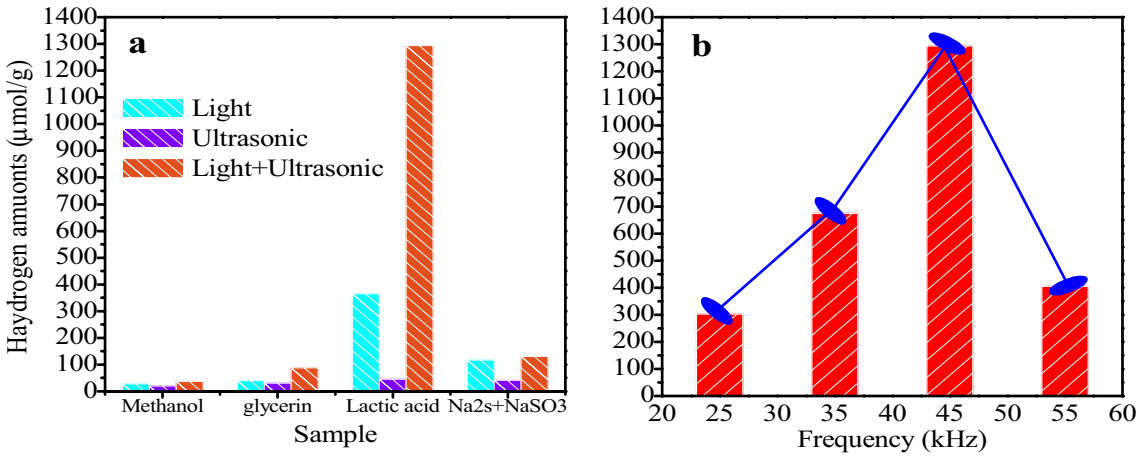

Fig. 8 **a** Photocatalytic activity of hydrogen production of 4-CdS square nanosheet sample by using different sacrificial agents (including 10% methanol, 10% glycerin, 10% lactic acid and 0.35 M Na_2S, 0.2 5 M Na_2SO_3), **b**The frequency-dependent difference of H_2-generation amount normalized by acoustic intensity

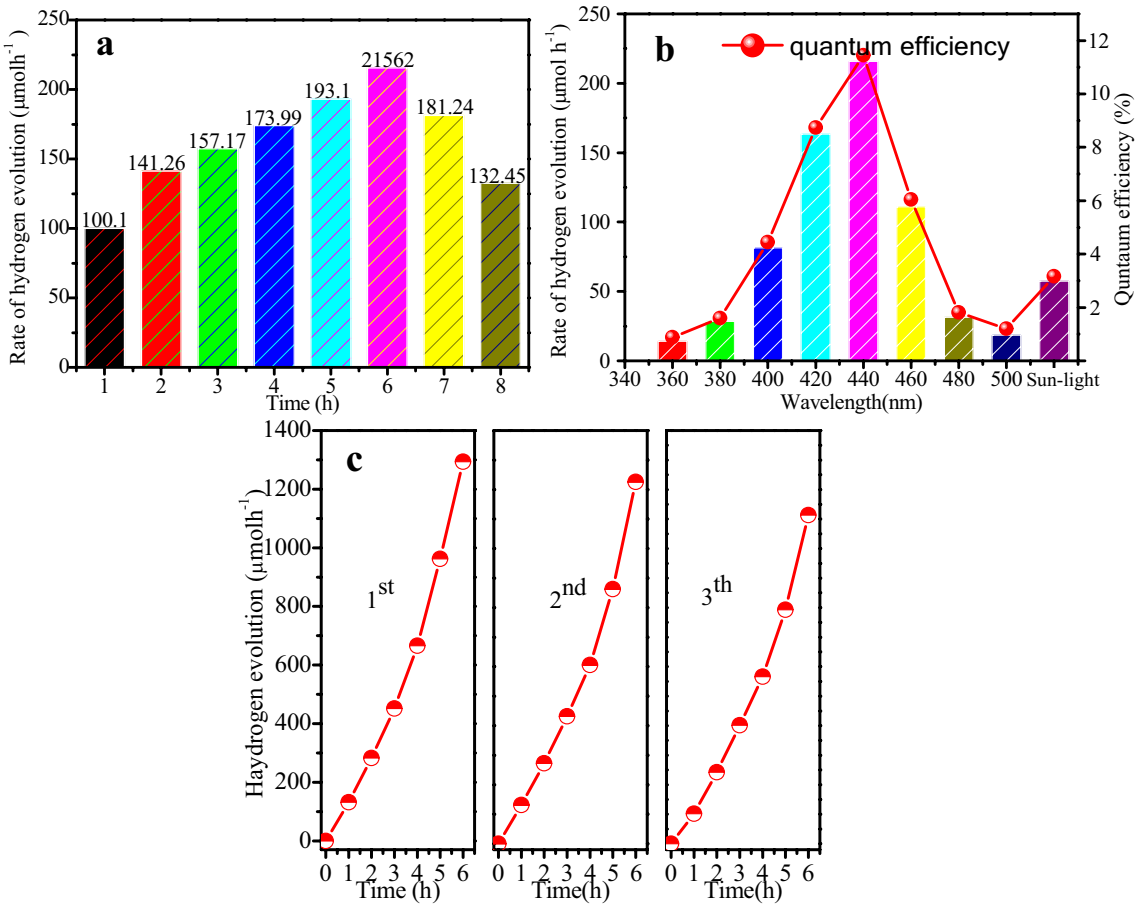

Fig. 9 **a** Photocatalytic activity of hydrogen production over the 4-CdS square nanosheets for 1, 2, 3, 4. 5, 6, 7 and 8 h, respectively. **b** The hydrogen evolution rate and quantum efficiency of 4-CdS under monochromatic light irradiation. **c** Cyclic hydrogen production of 4-CdS under visible light irradiation

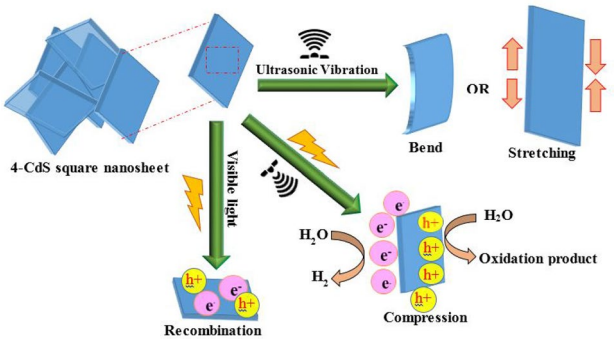

Fig. 10 Schematic illustration for phot0/piezo-bi-catalytic mechanism of the 4-CdS square nanosheets

the 4-CdS nanosheets for H_2 evolution due to the significance of the photostability of these nanosheets in enhancing practical applications. As shown in Fig. 8, the H_2-production rate in the 4-CdS nanosheets gradually decrease after each reaction period. After three consecutive recycles, the 4-CdS sample lost 12% of its initial catalytic H_2-production activity under visible light. This result suggests that the 4-CdS photocatalysts exhibit good stability during photo-catalytic reaction. The activity loss can be due to the photo-corrosion of the as-prepared square CdS nanosheets by decreasing of lattice stress and holes [53–55]. Similar anomalies have been checked over CdS [56]. Moreover, Fig. SV (Supporting Information) presents the optimization amount of the 4-CdS photocatalyst and sacrificial agent.

From all the preceding results, a possible synergetic piezo-/photocatalysis mechanism for the square 4-CdS nanosheets was proposed and illustrated in Fig. 10. When irradiated by visible light, photo-induced holes and electrons can be formed in the valence band and the conduction band respectively, of the square 4-CdS nanosheet. However, low photocatalytic activity occurs because of the rapid recombination of (e^-–h^+) carriers consisting of surface and bulk recombination's [57]. When a periodic force resulting from mechanical force (ultrasound vibration) in water is introduced into square 4-CdS nanosheets, two potential types of deformation occurred on the nanosheets. One type is vertical compression or stretching and the other type is horizontal bending. The deformation of the square 4-CdS nanosheets resulted in the production of a many negative and positive charges on the surfaces of the sheets due to the piezoelectric effect of CdS. Increase deformation of the energy band (regardless of the type) should allow the transfer of photogenerated holes and electrons. When light and ultrasonic waves are simultaneously applied, the nanosheets generate an electrical field with the positive electrode facing down. Under this electric field, the photogenerated hole move toward the top surface, and the electrons migrate towered the bottom surface to increase regional electron density on the surface of the CdS nanosheet. The catalytic activity of 4-CdS increases significantly under solar and ultrasonic vibrations compared to the 0-CdS and other prepared samples. This result confirms the explanation that the improvement of photoactivity can be due to an increase of surface area and the charge separation induced by the synergetic effect of light and ultrasound.

4 Conclusion

In summary, an easy method for constructing CdS nanosheets with the thickness setting controlled by DL-dithiothreitol amount was identified in this report. The influence of sheet thickness on photocatalytic hydrogen generation was discussed. Compared with ultrasonic vibration or light irradiation alone, the coupling of ultrasound and light can simulate the combined effects of the photo/piezoelectric field, making water dissociation considerably easier catalyze to produce H_2. Considering the aforementioned facts, the obtained square-like CdS nanosheets with a thickness of 28 nm exhibited an exceptional photo/piezo-bi-catalytic H_2 production activity of 1293.62 μmol g^{-1} h^{-1} and accomplished an apparent quantum efficiency of 11.72% in H_2 generation. The hydrogen proportion generated under the synergistic effect was more than four times the imposition of vibration and light. This work demonstrates that the thickness of CdS nanosheets and the piezoelectric field exert an impact on shortening the time of electrons-holes recombination, significant increasing photocatalytic water splitting for H_2 generation.

References

1. Ganguly P, Harb M, Cao Z et al (2019) 2D Nanomaterials for Photocatalytic Hydrogen Production. ACS Energy Lett 4:1687–1709. https://doi.org/10.1021/acsenergylett.9b00940
2. Finegold L, Cude JL (1972) Biological sciences: One and two-dimensional structure of alpha-helix and beta-sheet forms of poly(L-Alanine) shown by specific heat measurements at low temperatures (1.5-20 K). Nature 238:38–40. https://doi.org/10.1038/238038a0
3. Wen J, Li X, Liu W et al (2015) Photocatalysis fundamentals and surface modification of TiO2 nanomaterials. Cuihua Xuebao/Chinese J Catal 36:2049–2070. https://doi.org/10.1016/S1872-2067(15)60999-8
4. Wen J, Xie J, Chen X, Li X (2017) A review on g-C 3 N 4 -based photocatalysts. Appl Surf Sci 391:72–123. https://doi.org/10.1016/j.apsusc.2016.07.030
5. Hu T, Dai K, Zhang J et al (2019) Noble-metal-free Ni2P as cocatalyst decorated rapid microwave solvothermal synthesis of inorganic-organic CdS-DETA hybrids for enhanced photocatalytic hydrogen evolution. Appl Surf Sci 481:1385–1393
6. Ren D, Shen R, Jiang Z et al (2020) Highly efficient visible-light photocatalytic H2 evolution over 2D–2D CdS/Cu7S4 layered heterojunctions. Chinese J Catal 41:31–40

7. Yu W, Zhang S, Chen J et al (2018) Biomimetic Z-scheme photocatalyst with a tandem solid-state electron flow catalyzing H_2 evolution. J Mater Chem A 6:15668–15674
8. Zhou FQ, Fan JC, Xu QJ, Min YL (2017) BiVO4 nanowires decorated with CdS nanoparticles as Z-scheme photocatalyst with enhanced H2 generation. Appl Catal B 201:77–83. https://doi.org/10.1016/j.apcatb.2016.08.027
9. Fang Z, Wang Y, Song J et al (2013) Immobilizing CdS quantum dots and dendritic Pt nanocrystals on thiolated graphene nanosheets toward highly efficient photocatalytic H2 evolution. Nanoscale 5:9830–9838. https://doi.org/10.1039/c3nr03043a
10. Yin S, Han J, Zou Y et al (2016) A highly efficient noble metal free photocatalytic hydrogen evolution system containing MoP and CdS quantum dots. Nanoscale 8:14438–14447. https://doi.org/10.1039/c6nr00989a
11. Yu J, Yu Y, Cheng B (2012) Enhanced visible-light photocatalytic H 2-production performance of multi-armed CdS nanorods. RSC Adv 2:11829–11835. https://doi.org/10.1039/c2ra22019a
12. He K, Wang M, Guo L (2015) Novel-CdS-nanorod with stacking fault structures: Preparation and properties of visible-light-driven photocatalytic hydrogen production from water. Chem Eng J 279:747–756. https://doi.org/10.1016/j.cej.2015.04.069
13. Kim W, Monllor-Satoca D, Chae WS et al (2019) Enhanced photoelectrochemical and hydrogen production activity of aligned CdS nanowire with anisotropic transport properties. Appl Surf Sci 463:339–347. https://doi.org/10.1016/j.apsusc.2018.08.127
14. Jang JS, Joshi UA, Lee JS (2007) Solvothermal synthesis of CdS nanowires for photocatalytic hydrogen and electricity production. J Phys Chem C 111:13280–13287. https://doi.org/10.1021/jp072683b
15. Garg P, Bhauriyal P, Mahata A et al (2019) Role of dimensionality for photocatalytic water splitting: cds nanotube versus bulk structure. ChemPhysChem. https://doi.org/10.1002/cphc.201801051
16. Ju L, Dai Y, Wei W et al (2018) One-dimensional cadmium sulphide nanotubes for photocatalytic water splitting. Phys Chem Chem Phys 20:1904–1913. https://doi.org/10.1039/c7cp06568j
17. Xu Y, Zhao W, Xu R et al (2013) Synthesis of ultrathin CdS nanosheets as efficient visible-light-driven water splitting photocatalysts for hydrogen evolution. Chem Commun 49:9803–9805. https://doi.org/10.1039/c3cc46342g
18. Ning X, Wu Y, Ma X et al (2019) A novel charge transfer channel to simultaneously enhance photocatalytic water splitting activity and stability of CdS. Adv Funct Mater 29:1–9. https://doi.org/10.1002/adfm.201902992
19. Cheng L, Xiang Q, Liao Y, Zhang H (2018) CdS-based photocatalysts. Energy Environ Sci 11:1362–1391. https://doi.org/10.1039/c7ee03640j
20. Di T, Zhu B, Zhang J et al (2016) Enhanced photocatalytic H2 production on CdS nanorod using cobalt-phosphate as oxidation cocatalyst. Appl Surf Sci 389:775–782
21. Zou J, Cao Y, Sun Y et al (2018) A comparative study of the photoconduction, photocatalytic and electrocatalytic performance of gC 3 N 4/ZnS/CuS heterojunctions with different morphologies. Catal Letters 148:3342–3348
22. Yang Y, Zhang D, Xiang Q (2019) Plasma-modified Ti 3 C 2 T x/CdS hybrids with oxygen-containing groups for high-efficiency photocatalytic hydrogen production. Nanoscale 11:18797–18805
23. Yan X, Xu B, Yang X et al (2019) Through hydrogen spillover to fabricate novel 3DOM-HxWO3/Pt/CdS Z-scheme heterojunctions for enhanced photocatalytic hydrogen evolution. Appl Catal B 256:117812. https://doi.org/10.1016/j.apcatb.2019.117812
24. Ma Q, Peng X, Zhu M et al (2018) Strategic modulation of electron migration in the TiO2-Au-CdS: Z-scheme design for the enhancement in hydrogen evolution reaction. Electrochem Commun 95:28–32. https://doi.org/10.1016/j.elecom.2018.08.010
25. Zhang Y, Jin Z, Yan X et al (2019) Effect of Ni (OH) 2 on CdS@gC 3 N 4 composite for efficient photocatalytic hydrogen production. Catal Lett 149:1174–1185
26. Cheng L, Zhang D, Fan J et al (2020) Metal phosphide modified CdxZn1− xS solid solutions as a highly active visible-light photocatalyst for hydrogen evolution. Appl Catal A 590:117336
27. Li X, Yu J, Wageh S et al (2016) Graphene in photocatalysis: a review. Small 12:6640–6696. https://doi.org/10.1002/smll.201600382
28. Ranjan R, Sinha ASK (2019) Optimizations of r GO supported CdS photo-electrocatalyst for dissociation of water. Int J Hydrogen Energy 44:5955–5969. https://doi.org/10.1016/j.ijhydene.2019.01.112
29. Mu R, Ao Y, Wu T et al (2020) Synergistic effect of molybdenum nitride nanoparticles and nitrogen-doped carbon on enhanced photocatalytic hydrogen evolution performance of CdS nanorods. J Alloys Compd 812:151990. https://doi.org/10.1016/j.jallcom.2019.151990
30. Yan H, Yang J, Ma G et al (2009) Visible-light-driven hydrogen production with extremely high quantum efficiency on Pt-PdS/CdS photocatalyst. J Catal 266:165–168. https://doi.org/10.1016/j.jcat.2009.06.024
31. Liang Z, Yan CF, Rtimi S, Bandara J (2019) Piezoelectric materials for catalytic/photocatalytic removal of pollutants: recent advances and outlook. Appl Catal B Environ 241:256–269. https://doi.org/10.1016/j.apcatb.2018.09.028
32. Cheng L, Zhang D, Liao Y et al (2019) One-step solid-phase synthesis of 2D ultrathin CdS nanosheets for enhanced visible-light photocatalytic hydrogen evolution. Sol RRL 1900062:1900062. https://doi.org/10.1002/solr.201900062
33. Mushtaq F, Chen X, Hoop M et al (2018) Piezoelectrically Enhanced Photocatalysis with BiFeO3 Nanostructures for Efficient Water Remediation. iScience 4:236–246. https://doi.org/10.1016/j.isci.2018.06.003
34. Wang ZL (2012) Progress in piezotronics and piezo-phototronics. Adv Mater 24:4632–4646. https://doi.org/10.1002/adma.201104365
35. Yein WT, Wang Q, Li Y, Wu X (2019) Piezoelectric potential induced the improved micro-pollutant dye degradation of Co doped MoS2 ultrathin nanosheets in dark. Catal Commun 125:61–65. https://doi.org/10.1016/j.catcom.2019.03.023
36. Ismail M, Wu Z, Zhang L et al (2019) High-efficient synergy of piezocatalysis and photocatalysis in bismuth oxychloride nanomaterial for dye decomposition. Chemosphere 228:212–218. https://doi.org/10.1016/j.chemosphere.2019.04.121
37. Lin YF, Song J, Ding Y et al (2008) Alternating the output of a CdS nanowire nanogenerator by a white-light-stimulated optoelectronic effect. Adv Mater 20:3127–3130. https://doi.org/10.1002/adma.200703236
38. Hinchet R, Khan U, Falconi C, Kim SW (2018) Piezoelectric properties in two-dimensional materials: simulations and experiments. Mater Today 21:611–630. https://doi.org/10.1016/j.mattod.2018.01.031
39. Zhao Y, Bin FZ, Feng W et al (2018) Hydrogen production from pure water via piezoelectric-assisted visible-light photocatalysis of CdS nanorod arrays. ChemCatChem 10:3397–3401. https://doi.org/10.1002/cctc.201800666
40. Zhao Y, Huang X, Gao F et al (2019) Study on water splitting characteristics of CdS nanosheets driven by the coupling effect between photocatalysis and piezoelectricity. Nanoscale 11:9085–9090. https://doi.org/10.1039/c9nr01676g
41. Mi Y, Zhou M, Wen L et al (2014) A highly efficient visible-light driven photocatalyst: two dimensional square-like bismuth oxyiodine nanosheets. Dalt Trans 43:9549–9556. https://doi.org/10.1039/c4dt00798k

42. Wu A, Tian C, Jiao Y et al (2017) Sequential two-step hydrothermal growth of MoS2/CdS core-shell heterojunctions for efficient visible light-driven photocatalytic H2 evolution. Appl Catal B 203:955–963. https://doi.org/10.1016/j.apcatb.2016.11.009
43. Al Balushi BSM, Al Marzouqi F, Al Wahaibi B et al (2018) Hydrothermal synthesis of CdS sub-microspheres for photocatalytic degradation of pharmaceuticals. Appl Surf Sci 457:559–565. https://doi.org/10.1016/j.apsusc.2018.06.286
44. Jin J, Yu J, Liu G, Wong PK (2013) Single crystal CdS nanowires with high visible-light photocatalytic H 2-production performance. J Mater Chem A 1:10927–10934. https://doi.org/10.1039/c3ta12301d
45. Yu J, Yu Y, Zhou P et al (2014) Morphology-dependent photocatalytic H2-production activity of CdS. Appl Catal B 156–157:184–191. https://doi.org/10.1016/j.apcatb.2014.03.013
46. You D, Pan B, Jiang F et al (2016) CdS nanoparticles/CeO 2 nanorods composite with high-efficiency visible-light-driven photocatalytic activity. Appl Surf Sci 363:154–160. https://doi.org/10.1016/j.apsusc.2015.12.021
47. Li Y, Yang M, Xing Y et al (2017) Preparation of carbon-rich g-C3N4 nanosheets with enhanced visible light utilization for efficient photocatalytic hydrogen production. Small 13:1–8. https://doi.org/10.1002/smll.201701552
48. Abbood HA, Ahmed KAM, Ren Y, Huang K (2013) MnV2O6×V2O5 cross-like nanobelt arrays: synthesis, characterization and photocatalytic properties. Appl Phys A Mater Sci Process 112:901–909. https://doi.org/10.1007/s00339-012-7444-y
49. Sun Y, Gao S, Lei F, Xie Y (2015) Atomically-thin two-dimensional sheets for understanding active sites in catalysis. Chem Soc Rev 44:623–636. https://doi.org/10.1039/c4cs00236a
50. Xue C, Yan X, An H et al (2018) Applied catalysis B: environmental bonding CdS-Sn 2 S 3 eutectic clusters on graphene nanosheets with unusually photoreaction-driven structural reconfiguration effect for excellent H2 evolution and Cr (VI) reduction. Appl Catal B 222:157–166. https://doi.org/10.1016/j.apcatb.2017.10.008
51. Jyothi KP, Yesodharan S, Yesodharan EP (2014) Ultrasonics Sonochemistry ultrasound (US), ultraviolet light (UV) and combination (US + UV) assisted semiconductor catalysed degradation of organic pollutants in water: oscillation in the concentration of hydrogen peroxide formed in situ. Ultrason Sonochem. https://doi.org/10.1016/j.ultsonch.2014.03.019
52. Xu Y, Huang Y, Zhang B (2016) Rational design of semiconductor-based photocatalysts for advanced photocatalytic hydrogen production: The case of cadmium chalcogenides. Inorg Chem Front 3:591–615. https://doi.org/10.1039/c5qi00217f
53. Ning X, Lu G (2020) Photocorrosion inhibition of CdS-based catalysts for photocatalytic overall water splitting. Nanoscale 12:1213–1223. https://doi.org/10.1039/C9NR09183A
54. Nasir JA, Ambareen H, Khan A et al (2018) Photoreduction of 4-nitrophenol to 4-aminophenol using CdS nanorods. J Nanosci Nanotechnol 18:7516–7522. https://doi.org/10.1166/jnn.2018.16092Solar
55. Khan A, Khan A, Ambareen H et al (2017) light driven photocatalytic conversion of p-nitrophenol to p-aminophenol on CdS nanosheets and nanorods. Inorg Chem Commun 79:99–103. https://doi.org/10.1016/j.inoche.2017.03.033
56. Chandrasekaran S, Yao L, Deng L et al (2019) Recent advances in metal sulfides: from controlled fabrication to electrocatalytic, photocatalytic and photoelectrochemical water splitting and beyond. Chem Soc Rev 48:4178–4280. https://doi.org/10.1039/c8cs00664d
57. Zhou M, Chen J, Hou C et al (2019) Organic-free synthesis of porous CdS sheets with controlled windows size on bacterial cellulose for photocatalytic degradation and H 2 production. Appl Surf Sci 470:908–916. https://doi.org/10.1016/j.apsusc.2018.11.207

Affiliations

Hayder A. Abbood[1,2] · Akram Alabadi[3] · Adnan B. Al-Hawash[4] · Anwar A. Abbood[1,2,3,4,5] · Kaixun Huang[1,2]

✉ Hayder A. Abbood
hayder.abood@uobasrah.edu.iq

✉ Kaixun Huang
hxxzrf@mail.hust.edu.cn

[1] School of Chemistry and Chemical Engineering, Huazhong University of Science and Technology, Wuhan 430074, People's Republic of China

[2] Department of Material Engineering, College of Engineering, University of Basrah, Basrah, Iraq

[3] South Refineries Company, Ministry of Oil, Basra 61006, Iraq

[4] Department of Marine Chemistry and Environmental Pollution, Marine Science Centre, University of Basrah, Basrah, Iraq

[5] Department of Chemical Engineering, College of Engineering, University of Basrah, Basrah, Iraq